2004

LISA time-delay interferometry zero-signal solution: Geometrical properties

Massimo Tinto

Shane L. Larson
Utah State University

Recommended Citation
Massimo Tinto and Shane L. Larson, "The LISA time-delay interferometry zero-signal solution I: geometrical properties", Phys. Rev. D, 70 062002 (2004).

LISA time-delay interferometry zero-signal solution: Geometrical properties

Massimo Tinto*
Jet Propulsion Laboratory, California Institute of Technology, Pasadena, California 91109, USA

Shane L. Larson†
Space Radiation Laboratory, California Institute of Technology, Pasadena, California 91125, USA
(Received 29 May 2004; published 15 September 2004)

Time-delay interferometry (TDI) is the data processing technique needed for generating interferometric combinations of data measured by the multiple Doppler readouts available onboard the three Laser Interferometer Space Antenna (LISA) spacecraft. Within the space of all possible interferometric combinations TDI can generate, we have derived a specific combination that has zero response to the gravitational wave signal, and called it the *zero-signal solution* (ZSS). This is a two-parameter family of linear combinations of the generators of the TDI space, and its response to a gravitational wave becomes null when these two parameters coincide with the values of the angles of the source location in the sky. Remarkably, the ZSS does not rely on any assumptions about the gravitational waveform, and in fact it works for waveforms of any kind. Our approach is analogous to the data analysis method introduced by Gürsel and Tinto in the context of networks of Earth-based, wideband, interferometric gravitational wave detectors observing in coincidence a gravitational wave burst. The ZSS should be regarded as an application of the Gürsel and Tinto method to the LISA data.

DOI: 10.1103/PhysRevD.70.062002 PACS numbers: 04.80.Nn, 07.60.Ly, 95.55.Ym

I. INTRODUCTION

LISA, the Laser Interferometer Space Antenna, is a deep-space mission of three spacecraft flying in a triangular formation. Jointly proposed to the National Aeronautics and Space Administration and the European Space Agency, it aims to detect and study gravitational radiation in the millihertz frequency band via laser interferometry [1].

Modeling each spacecraft as carrying lasers, beam splitters, photodetectors, and drag-free proof masses on each of two optical benches, it has been shown [2–9] that the six measured time series of Doppler shifts of the one-way laser beams between spacecraft pairs, and the six measured shifts between adjacent optical benches on each spacecraft, can be combined, with suitable time delays, to cancel the otherwise overwhelming frequency fluctuations of the lasers ($\Delta\nu/\nu \simeq 10^{-13}/\sqrt{\mathrm{Hz}}$), and the noise due to the mechanical vibrations of the optical benches (which could be as large as $\Delta\nu/\nu \simeq 10^{-16}/\sqrt{\mathrm{Hz}}$). The achievable strain sensitivity level $h \simeq 10^{-21}/\sqrt{\mathrm{Hz}}$ is set by the buffeting of the drag-free proof masses inside each optical bench, and by the shot noise at the photodetectors.

In contrast to Earth-based, equal-arm interferometers for gravitational wave (GW) detection, LISA will have multiple readouts. The data they generate, when properly time shifted and linearly combined, provide observables that are not only insensitive to laser frequency fluctuations and optical bench motions, but at the same time show different couplings to gravitational radiation and to the remaining system noises. The technique for synthesizing all these interferometric combinations has been called time-delay interferometry (TDI), and it has been shown that the functional space it generates can be obtained by properly time shifting and linearly combining the four Sagnac generators ($\alpha, \beta, \gamma, \zeta$) [2,3,5,10]. In particular, there exists a combination of the four generators that, for a given waveform and source location in the sky, achieves maximum signal-to-noise ratio (SNR) [11].

Here we further elaborate on the geometrical properties of the four generators' responses. We find that there exists a two-parameter family of combinations of ($\alpha, \beta, \gamma, \zeta$) that has null response to an observed gravitational wave signal. In the case of gravitational wave bursts, or sinusoidal signals observed over a time scale short enough that the amplitude and frequency modulation induced on the received signal by the LISA motion around the Sun are negligible, this new TDI combination shows a sharp null when its two parameters coincide with the values of the angles describing the source location in the sky, or its mirror image with respect to the LISA plane. This combination, which we call the *zero-signal solution* (ZSS), does not rely on any assumptions about the gravitational waveform, and in fact it works for gravitational waveforms of any kind. Although its ability to identify these two points in the sky degrades at lower frequencies, it should be regarded as an improvement over the symmetric Sagnac combination, ζ [10], since it could be used for discriminating gravitational wave signals from spurious fluctuations generated by instrumental noise in the entire LISA frequency band.

*Also at: Space Radiation Laboratory, California Institute of Technology, Pasadena, CA 91125, USA.
Electronic address: Massimo.Tinto@jpl.nasa.gov
†Electronic address: shane@srl.caltech.edu

The ability of the ZSS to identify the source location in the sky follows from the fact that the time spent by the gravitational wave front to propagate across the LISA constellation enters into the gravitational wave responses of the four generators ($\alpha, \beta, \gamma, \zeta$). The two independent travel times spent by the wave to propagate from one spacecraft to the other two define the "six-pulse" [2] structure in the responses of the four generators. Since the signal contribution to the ZSS combination becomes null at the correct values of these two time delays, and the antenna pattern of the ZSS is symmetric with respect to the LISA plane, it follows that in general there are two possible points in the sky where the signal must have originated. If the duration of the signal is such that the effects of the motion of the LISA array around the Sun can be disregarded (as in the case of bursts), then the twofold degeneracy cannot be removed. However, if the duration of the signal is such that the effects of the motion of LISA around the solar system barycenter can be measured (as in the case of signals from binary systems), then the source location can be uniquely identified. As LISA moves around the Sun, the point in the sky where the source is located will remain fixed, while the other will move in such a way to remain its mirror image with respect to the LISA plane. By constructing the ZSS with different stretches of data, the unique source location can be identified.

The ability of the ZSS to identify two possible points in the sky where an observed gravitational wave signal must have come from will be particularly useful when observing gravitational wave bursts, or continuous signals that are strong enough to be observed by integrating the data over time scales shorter than the time scale during which the phase and amplitude modulations of the signal become measurable. In the latter case, the ZSS should be regarded as the first step of a hierarchical procedure for measuring the parameters of a continuous signal. The ZSS could be particularly useful when observing, for instance, gravitational radiation emitted during the inspiral of two supermassive black holes, or one smaller object into a supermassive hole. The ability of the ZSS to identify the location of the binary system in the sky, without relying on the knowledge of the signal waveform, might reduce significantly the number of templates needed in order to study waveforms from such astrophysical systems [12].

This paper is organized as follows. Section II provides a brief overview of time-delay interferometry, the data analysis technique needed to remove the frequency fluctuations of the six lasers and other noise sources affecting the LISA measurements. After showing that the entire space of interferometric combinations can be generated by properly combining the six-pulse Sagnac combinations ($\alpha, \beta, \gamma, \zeta$), in Sec. III we obtain the general expression of the ZSS in the Fourier domain, and note that it does not rely on any assumptions about the time dependence of the observed gravitational wave signal. The corresponding expression of the ZSS in the time domain is then given in Sec. IV, where we show that the three data sets, α, β, and γ, enter with 81 different time delays. Section V derives the expression of the ZSS in the long-wavelength approximation (i.e., when the characteristic wavelength of the wave is much larger than the typical linear size of the LISA array). In Sec. VI we give a summary of our work and emphasize that this "part I" article only addresses the geometrical properties of the ZSS. A quantitative analysis covering its ability to discriminate gravitational wave signals from random noise fluctuations affecting the LISA data, and the accuracies it will achieve in reconstructing the source location in the sky and the wave's two independent amplitudes, will be presented in a companion article.

II. SUMMARY OF TIME-DELAY INTERFEROMETRY FOR LISA

A brief overview of TDI, the technique needed to remove the frequency fluctuations of the lasers from phase measurements obtained with an unequal-arm interferometer, is presented in this section. The reader is referred to the articles [2–5,13] for a derivation of TDI valid for the nonrotating and rigid LISA configuration [the so-called "first generation TDI" (TDI1)], and to the following ones [6–9] for the modified expressions accounting for the LISA spacecraft motions [the "second generation" TDI (TDI2)]. The overall LISA geometry is shown in Fig. 1. There are six beams exchanged between the LISA spacecraft, with the six Doppler measurements y_{ij} ($i, j = 1, 2, 3$) recorded when each transmitted beam is mixed with the laser light of the receiving optical bench. The frequency fluctuations from the six lasers, which enter in each of the six Doppler measurements, need to be suppressed to a level smaller than that identified by the secondary (proof mass and optical path) noises [1] in order to detect and study gravitational radiation at the predicted amplitudes.

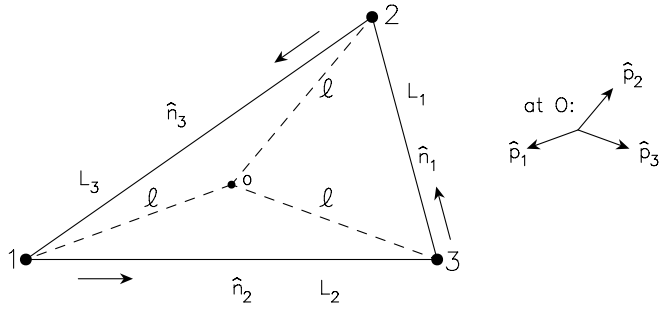

FIG. 1. Schematic LISA configuration. Each spacecraft is equidistant from point o, with unit vectors $\hat{p}_i$ indicating directions to the three spacecraft. Unit vectors $\hat{n}_i$ point between spacecraft pairs with the indicated orientation.

Since the LISA triangular array has systematic motions, the two one-way light times between any spacecraft pair are not the same [6]. Delay times for travel between the spacecraft must be accounted for depending on the sense of light propagation along each link when combining these data as a consequence of the rotation of the array. Following [9], the arms are labeled with single numbers given by the opposite spacecraft; e.g., arm 2 (or $2'$) is opposite spacecraft 2, where primed delays are used to distinguish light times taken in the counterclockwise sense and unprimed delays for the clockwise light times (see Fig. 2). Also the following labeling convention of the Doppler data will be used. Explicitly: y_{23} is the one-way Doppler shift measured at spacecraft 3, coming from spacecraft 2, along arm 1. Similarly, y_{32} is the Doppler shift measured on arrival at spacecraft 2 along arm $1'$ of a signal transmitted from spacecraft 3. Because of the relative motion between spacecraft, $L_1 \neq L_1'$ in general. As in [3,4], we denote six further data streams, z_{ij} ($i, j = 1, 2, 3$), as the intraspacecraft metrology data used to monitor the motion of the two optical benches and the relative phase fluctuations of the two lasers on each of the three spacecraft. Finally, the light times L_i and L_i' ($i = 1, 2, 3$) are not only different (pure rotation) but also change in time. For this reason, in the subscript notation for delays, their *order* is important [7–9]. The frequency fluctuations introduced by the gravitational wave signal, the lasers, the optical benches, the proof masses, the fiber optics, and the measurement itself at the photodetector (shot noise) enter into the Doppler observables y_{ij}, z_{ij} with specific time signatures. They have been derived in the literature [3,4], and we refer the reader to those papers for a detailed discussion. The Doppler data y_{ij}, z_{ij} are the fundamental measurements needed to synthesize all the interferometric observables unaffected by laser and optical bench noises.

Let us consider the TDI2 Sagnac observables: (ρ_1, ρ_2, ρ_3) [14]. Their expressions in terms of the Doppler measurements y_{ij}, z_{ij} are as follows [8]:

$$\begin{aligned}\rho_1 = {} & [y_{31} + y_{23;2} + y_{12;12} + y_{21;312} + y_{32;3'312} + y_{13;1'3'312}] - [y_{21} + y_{32;3'} + y_{13;1'3'} + y_{31;2'1'3'} + y_{23;22'1'3'} + y_{12;122'1'3'}] \\ & + \tfrac{1}{2}[(z_{21} - z_{31}) - (z_{21} - z_{31})_{;2'1'3'312} + (z_{32} - z_{12})_{;3'} + (z_{32} - z_{12})_{;12} - (z_{32} - z_{12})_{;3'312} - (z_{32} - z_{12})_{;122'1'3'} + (z_{13} \\ & - z_{23})_{;2} + (z_{13} - z_{23})_{;1'3'} - (z_{13} - z_{23})_{;22'1'3'} - (z_{23} - z_{13})_{;1'3'312}],\end{aligned} \tag{1}$$

with ρ_2, ρ_3 following from Eq. (1) by permutations of the spacecraft indices. The semicolon notation shown in Eq. (1) emphasizes that the operation of sequentially applying two or more delays to a given measurement is noncommutative, and a specific order has to be adopted to adequately suppress the laser noises [8,9]. Specifically: $y_{ij;kl} \equiv y_{ij}[t - L_l(t) - L_k(t - L_l)] \neq y_{ij;lk}$.

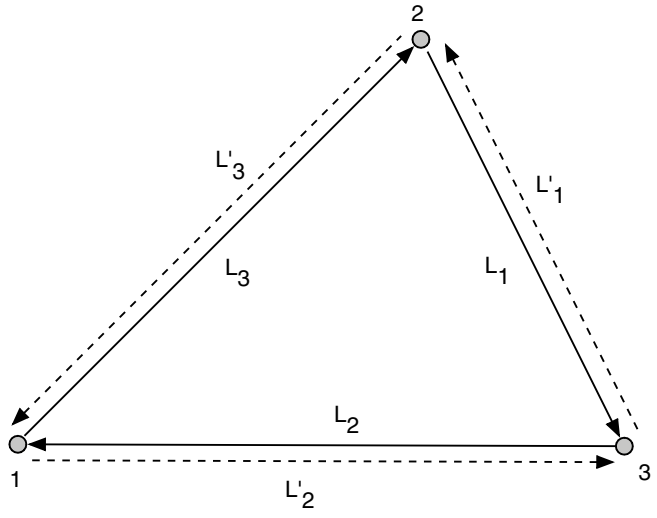

FIG. 2. Schematic diagram of LISA configurations involving six laser beams. Optical path delays taken in the counterclockwise sense are denoted with a prime, while unprimed delays are in the clockwise sense.

The expressions of the gravitational wave signal and the secondary noise sources entering into ρ_1 will in general be different from those entering into α, the corresponding Sagnac observable derived under the assumption of a stationary LISA array [2,3]. However, the other remaining, secondary noises in LISA are so much smaller, and the rotation and systematic velocities in LISA are so intrinsically small, that index permutation may still be done for them [9]. It is therefore easy to derive the following relationship between the signal and secondary noises in ρ_1, and those entering into the TDI1 combination α [8,9]:

$$\rho_1(t) \simeq \alpha(t) - \alpha(t - L_1 - L_2 - L_3), \tag{2}$$

where L_i, $i = 1, 2, 3$ are the unequal-arm lengths of the stationary LISA array. Equation (2) implies that any data analysis procedure and algorithm that will be implemented for the TDI2 combinations can actually be derived by considering the corresponding TDI1 combinations. For this reason, from now on we will focus our attention on the gravitational wave responses of the TDI1 observables $(\alpha, \beta, \gamma, \zeta)$ [2,3].

In the reference frame comoving with LISA and centered at the point o that is equidistant from the three spacecraft (see Fig. 3), the response of α to a gravitational wave signal is given by the following expression [2]:

$$\alpha^{gw} = \left[1 - \frac{l}{L_1}(\mu_2 - \mu_3)\right][\Psi_1(t - \mu_2 l - L_1 - L_2) - \Psi_1(t - \mu_3 l - L_2)] - \left[1 + \frac{l}{L_1}(\mu_2 - \mu_3)\right][\Psi_1(t - \mu_3 l - L_1 - L_3) - \Psi_1(t - \mu_2 l - L_3)] + \left[1 - \frac{l}{L_2}(\mu_3 - \mu_1)\right][\Psi_2(t - \mu_3 l - L_2) - \Psi_2(t - \mu_1 l)] - \left[1 + \frac{l}{L_2}(\mu_3 - \mu_1)\right][\Psi_2(t - \mu_1 l - L_2 - L_1 - L_3) - \Psi_2(t - \mu_3 l - L_1 - L_3)] + \left[1 - \frac{l}{L_3}(\mu_1 - \mu_2)\right][\Psi_3(t - \mu_1 l - L_3 - L_1 - L_2) - \Psi_3(t - \mu_2 l - L_1 - L_2)] - \left[1 + \frac{l}{L_3}(\mu_1 - \mu_2)\right][\Psi_3(t - \mu_2 l - L_3) - \Psi_3(t - \mu_1 l)]. \quad (3)$$

Here $\mu_i = \hat{k} \cdot \hat{p}_i$, with $\hat{p}_i$, $i = 1, 2, 3$ being the unit vector pointing from o to spacecraft i, and $\hat{k}$ the unit propagation vector of the wave. The function Ψ_i is equal to [2]

$$\Psi_i(t) = \frac{1}{2}\frac{\hat{n}_i \cdot \mathbf{h}(t) \cdot \hat{n}_i}{1 - (\hat{k} \cdot \hat{n}_i)^2}, \quad (4)$$

where $\mathbf{h}(t)$ is the first order spatial metric perturbation at point o. Note that $L_1 \hat{k} \cdot \hat{n}_1 = l(\mu_2 - \mu_3)$, and so forth by cyclic permutation of the indices. The gravitational wave $\mathbf{h}(t)$ can be written as $[h_+(t)\mathbf{e}_+ + h_\times(t)\mathbf{e}_\times]$, where the 3-tensors $\mathbf{e}_+$ and $\mathbf{e}_\times$ are transverse to $\hat{k}$ and traceless. With respect to an orthonormal propagation frame (x', y', z') their components are equal to

$$\mathbf{e}_+ = \begin{pmatrix} 1 & 0 & 0 \\ 0 & -1 & 0 \\ 0 & 0 & 0 \end{pmatrix}, \qquad \mathbf{e}_\times = \begin{pmatrix} 0 & 1 & 0 \\ 1 & 0 & 0 \\ 0 & 0 & 0 \end{pmatrix}. \quad (5)$$

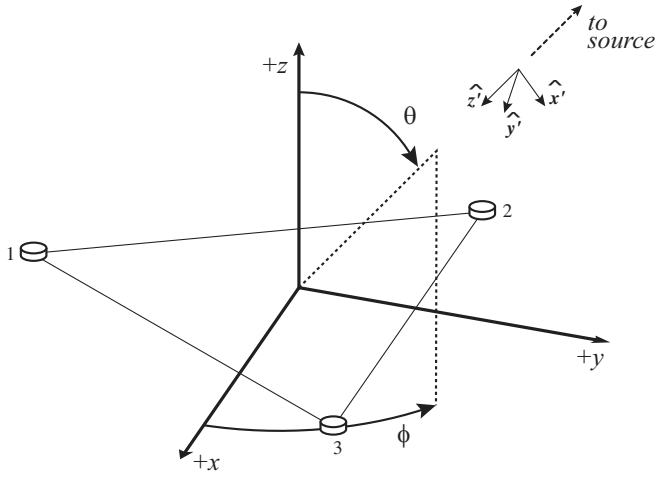

FIG. 3. The array and the wave coordinates. The x, y, and z axes are the LISA coordinate axes with the origin at the point o, and the array lies in the x, y plane. The x', y', z' axes are the coordinate axes for the incoming gravitational wave. The z' axis is parallel to the direction of propagation of the wave. The x', y' axes are those with respect to which $h_+(t)$ and $h_\times(t)$ are defined. The angles θ, ϕ describe the location of the source in the sky.

Equation (3) for α^{gw} shows a "six-pulse response" to gravitational radiation. In other words, a δ-function gravitational wave signal produces six distinct pulses in (α, β, γ) [2], which are located with relative times depending on the arrival direction of the wave and the detector configuration.

Together with (α, β, γ), the symmetric Sagnac combination, ζ, has been shown to form a basis for the TDI1 space of combinations and, like α, has a six-pulse response to gravitational radiation. Furthermore, it can be written in terms of (α, β, γ) in the following way [2]:

$$\zeta - \zeta_{,123} = \alpha_{,1} - \alpha_{,23} + \beta_{,1} - \beta_{,23} + \gamma_{,1} - \gamma_{,23}. \quad (6)$$

The four interferometric combinations $(\alpha, \beta, \gamma, \zeta)$ jointly also give the expressions of the interferometric combinations derived in [2,3]: the unequal-arm Michelson (X, Y, Z), the Beacon (P, Q, R), the Monitor (E, F, G), and the Relay (U, V, W) responses

$$X_{,1} = \alpha_{,23} - \beta_{,2} - \gamma_{,3} + \zeta, \quad (7)$$

$$P = \zeta - \alpha_{,1}, \quad (8)$$

$$E = \alpha - \zeta_{,1}, \quad (9)$$

$$U = \gamma_{,1} - \beta. \quad (10)$$

The remaining expressions can of course be obtained from Eqs. (7)–(10) by permutation of the spacecraft indices. All these interferometric combinations have been shown to add robustness to the mission with respect to failures of subsystems, and potential design, implementation, or cost advantages [2,3].

One important property of the ζ combination [10] is that it is much less sensitive to gravitational waves than any of the other Sagnac combinations (α, β, γ) in the low part of the frequency band accessible to LISA ($f \lesssim 5$ mHz). Since, however, it is affected by the same instrumental noise sources, it was recognized that it can be used as a "gravitational wave shield" for estimating the spectra of the instrumental noises affecting the "sensitive" combinations [10,15].

Although the ζ combination will be a very useful tool for assessing the on-flight-noise performance of LISA [10,15], it has been shown from first principles [11,16] that there exist a unique TDI combination that completely suppresses an observed gravitational wave signal incoming from a specific direction. In what follows we will derive the explicit analytic expression of such a combination.

III. THE ZSS IN THE FOURIER DOMAIN

LISA has the capability to *simultaneously* observe a gravitational wave signal with several interferometric combinations of different antenna patterns and noise transfer functions [3]. For this reason it should be regarded as an overlapping array of interferometric gravitational wave detectors working in coincidence. For a given signal waveform and source location in the sky, it has in fact been shown [11] that there exists an *optimal* combination of the generators of the TDI space that achieves maximum SNR.

In what follows we will answer a complementary question to the one addressed in [11]. We will identify, within the LISA TDI functional space, a specific interferometric combination that has zero response (and therefore zero SNR) to a gravitational wave signal. Such a combination provides a way for discriminating a gravitational wave signal from noise-generated fluctuations, and for this reason it should be regarded as an improvement over the symmetric Sagnac combination ζ [10].

Our approach is closely related to the one introduced by Gürsel and Tinto [17] in the context of data analysis for networks of ground-based interferometers observing in coincidence a gravitational wave burst. There, a network of three ground-based, wideband, detectors widely separated on the Earth was shown to provide enough information for uniquely solving the "inverse problem" in gravitational wave astronomy: the reconstruction of the wave's two independent amplitudes and the determination of the location of the wave source in the sky. With three noncoplanar detector responses and two independent time delays, it is possible to identify a unique, two-parameter linear combination of the three independent detector measurements that has zero response to the gravitational wave signal when the two parameters coincided with the values of the polar angles of the source location in the sky [17].

For LISA there exists an analogous two-parameter linear combination of the four generators of the TDI space, $(\alpha, \beta, \gamma, \zeta)$, which in the high-frequency part of the LISA band is capable of identifying two points in the sky where the observed gravitational wave burst must have come from. The property of this combination, which we have named the zero-signal solution, follows from the fact that the two independent travel times spent by the burst propagating across the three spacecraft define the separation of the six pulses in the responses of the four generators $(\alpha, \beta, \gamma, \zeta)$ [2]. Each travel time defines a circle on the sky where the signal must have come from, and their intersection reduces the source location to two possible points. However, due to the coplanarity of the antenna patterns of the four generators, the LISA ZSS is unable to resolve the two-solution ambiguity for bursts, as was possible with networks of three Earth-based laser interferometers [17].

In order to derive the expression of the ZSS, let us consider in the Fourier domain an arbitrary element of the TDI space, which we will refer to as $\tilde{\eta}$

$$\tilde{\eta}(f) \equiv a_1(f, \vec{\lambda})\tilde{\alpha}(f) + a_2(f, \vec{\lambda})\tilde{\beta}(f) + a_3(f, \vec{\lambda})\tilde{\gamma}(f) + a_4(f, \vec{\lambda})\tilde{\zeta}(f), \tag{11}$$

where the $\{a_i(f, \vec{\lambda})\}_{i=1}^4$ are arbitrary complex functions of the Fourier frequency f, and of a vector $\vec{\lambda}$ containing parameters characterizing the gravitational wave signal (source location in the sky, waveform parameters, etc.) and the noises affecting the four responses (noise levels, their correlations, etc.). For a given choice of the four functions $\{a_i\}_{i=1}^4$, $\tilde{\eta}$ gives an element of the functional space of interferometric combinations generated by $(\alpha, \beta, \gamma, \zeta)$. The corresponding expression of the signal-to-noise ratio, SNR_η^2, of the combination $\tilde{\eta}$ is equal to

$$\mathrm{SNR}_\eta^2 = \int_{f_l}^{f_u} \frac{|a_1\tilde{\alpha}_s + a_2\tilde{\beta}_s + a_3\tilde{\gamma}_s + a_4\tilde{\zeta}_s|^2}{\langle |a_1\tilde{\alpha}_n + a_2\tilde{\beta}_n + a_3\tilde{\gamma}_n + a_4\tilde{\zeta}_n|^2 \rangle} df. \tag{12}$$

In Eq. (12) the subscript n refers to the noise part of $(\tilde{\alpha}, \tilde{\beta}, \tilde{\gamma}, \tilde{\zeta})$, the angle brackets represent noise ensemble averages, and the interval of integration (f_l, f_u) corresponds to the frequency band accessible by LISA. As a consequence of the relationship between ζ and α, β, and γ [Eq. (6)], it has been shown [see Eq. (10) of Ref. [11]] that Eq. (12) can be rewritten in the following equivalent form:

$$\mathrm{SNR}_\eta^2 = \int_{f_l}^{f_u} \frac{|a_1\tilde{\alpha}\tilde{\alpha}^{gw} + a_2\tilde{\beta}^{gw} + a_3\tilde{\gamma}^{gw}|^2}{\langle |a_1\tilde{\alpha}_n + a_2\tilde{\beta}_n + a_3\tilde{\gamma}_n|^2 \rangle} df. \tag{13}$$

For a given choice of the three functions $\{a_i\}_{i=1}^3$, SNR_η^2 gives the corresponding SNR of an element of the TDI space, whose Fourier transform is equal to $\tilde{\eta} \equiv a_1\tilde{\alpha} + a_2\tilde{\beta} + a_3\tilde{\gamma}$. Our goal is therefore to identify, for a given gravitational wave signal, the three functions $\{a_i\}_{i=1}^3$ that give $\mathrm{SNR}_\eta^2 = 0$. Since SNR_η^2 is a positive definite functional, it can be zero if and only if the numerator of its integrand is identically null, i.e.,

$$\tilde{\eta}^{gw}(f) \equiv a_1\tilde{\alpha}^{gw}(f) + a_2\tilde{\beta}^{gw}(f) + a_3\tilde{\gamma}^{gw}(f) = 0. \tag{14}$$

The expressions for α^{gw}, β^{gw} and γ^{gw} can be rewritten in the following form [see Eqs. (3) and (4), and

Appendix B]:

$$\tilde{\alpha}^{gw}(f) = \alpha_+(f, \theta_s, \phi_s)\tilde{h}_+(f) + \alpha_\times(f, \theta_s, \phi_s)\tilde{h}_\times(f), \tag{15}$$

$$\tilde{\beta}^{gw}(f) = \beta_+(f, \theta_s, \phi_s)\tilde{h}_+(f) + \beta_\times(f, \theta_s, \phi_s)\tilde{h}_\times(f), \tag{16}$$

$$\tilde{\gamma}^{gw}(f) = \gamma_+(f, \theta_s, \phi_s)\tilde{h}_+(f) + \gamma_\times(f, \theta_s, \phi_s)\tilde{h}_\times(f), \tag{17}$$

where (θ_s, ϕ_s) are the two angles describing the location of the source in the sky with respect to a LISA coordinate frame (see Fig. 3), and the functions α_+, $\alpha_\times$, β_+, $\beta_\times$, γ_+, $\gamma_\times$ are pattern functions, derived in Appendix B. From these considerations it follows that $\tilde{\eta}^{gw}$ can be rewritten in the following form:

$$\begin{aligned}\tilde{\eta}^{gw}(f) = [&a_1\alpha_+(f, \theta_s, \phi_s) + a_2\beta_+(f, \theta_s, \phi_s) \\ &+ a_3\gamma_+(f, \theta_s, \phi_s)]\tilde{h}_+(f) + [a_1\alpha_\times(f, \theta_s, \phi_s) \\ &+ a_2\beta_\times(f, \theta_s, \phi_s) + a_3\gamma_\times(f, \theta_s, \phi_s)]\tilde{h}_\times(f),\end{aligned} \tag{18}$$

which is obtained by substituting Eqs. (15)–(17) into Eq. (14). The wave's two independent amplitudes, h_+, $h_\times$, are referred to the wave axes (x', y') which, without loss of generality, can be assumed to be oriented in such a way that the x' axis lies parallel to the LISA plane (the x-y plane). In order to have $\tilde{\eta}^{gw} = 0$ for any arbitrary pairs of wave's amplitudes h_+, $h_\times$, Eq. (18) implies that the following homogeneous linear system of two equations in three unknowns must be satisfied:

$$a_1\alpha_+(f, \theta_s, \phi_s) + a_2\beta_+(f, \theta_s, \phi_s) + a_3\gamma_+(f, \theta_s, \phi_s) = 0, \tag{19}$$

$$a_1\alpha_\times(f, \theta_s, \phi_s) + a_2\beta_\times(f, \theta_s, \phi_s) + a_3\gamma_\times(f, \theta_s, \phi_s) = 0. \tag{20}$$

Since the rank of the matrix associated with the linear system above is in general equal to 2, it is easy to derive the expressions for a_1, a_2, a_3 that give zero response to a gravitational wave signal at the source location

$$\begin{aligned}a_1(f, \theta_s, \phi_s) = &\beta_+(f, \theta_s, \phi_s)\gamma_\times(f, \theta_s, \phi_s) \\ &- \beta_\times(f, \theta_s, \phi_s)\gamma_+(f, \theta_s, \phi_s),\end{aligned} \tag{21}$$

$$\begin{aligned}a_2(f, \theta_s, \phi_s) = &\gamma_+(f, \theta_s, \phi_s)\alpha_\times(f, \theta_s, \phi_s) \\ &- \gamma_\times(f, \theta_s, \phi_s)\alpha_+(f, \theta_s, \phi_s),\end{aligned} \tag{22}$$

$$\begin{aligned}a_3(f, \theta_s, \phi_s) = &\alpha_+(f, \theta_s, \phi_s)\beta_\times(f, \theta_s, \phi_s) \\ &- \alpha_\times(f, \theta_s, \phi_s)\beta_+(f, \theta_s, \phi_s).\end{aligned} \tag{23}$$

Equations (21)–(23) imply that the following linear combination of the Fourier transforms of the three generators (α, β, γ)

$$\begin{aligned}\tilde{\eta} \equiv &[\beta_+(f, \theta, \phi)\gamma_\times(f, \theta, \phi) - \beta_\times(f, \theta, \phi)\gamma_+(f, \theta, \phi)]\tilde{\alpha}(f) \\ &+ [\gamma_+(f, \theta, \phi)\alpha_\times(f, \theta, \phi) \\ &- \gamma_\times(f, \theta, \phi)\alpha_+(f, \theta, \phi)]\tilde{\beta}(f) \\ &+ [\alpha_+(f, \theta, \phi)\beta_\times(f, \theta, \phi) \\ &- \alpha_\times(f, \theta, \phi)\beta_+(f, \theta, \phi)]\tilde{\gamma}(f)\end{aligned} \tag{24}$$

is a function of the two parameters (θ, ϕ), and it has null response to the gravitational wave signal observed in (α, β, γ) when $(\theta, \phi) \to (\theta_s, \phi_s)$, regardless of the particular waveform considered.

Note that the expression of $\tilde{\eta}^{gw}$ given in Eq. (24) changes sign under reflection with respect to the LISA plane. This is because the functions α_+, β_+, γ_+ are invariant under reflection with respect to the LISA plane, while $\alpha_\times$, $\beta_\times$, $\gamma_\times$ change sign under the same operation (see Appendices A and B for the derivation of these symmetry properties). This implies that the combinations $\alpha_+\beta_\times - \alpha_\times\beta_+$, $\beta_+\gamma_\times - \beta_\times\gamma_+$, $\gamma_+\alpha_\times - \gamma_\times\alpha_+$, which define the ZSS $\tilde{\eta}$, also change sign under reflection with respect to the LISA plane. In the case of a gravitational wave burst, or if we assume to observe a periodic signal for time scales shorter than the time during which the Doppler effect induced by the LISA motion around the Sun begins to be observable, we conclude that the ZSS will not be able to distinguish between the source location in the sky and the point that is its mirror image with respect to the LISA plane.

In the specific case of a sinusoidal signal, for which the two independent polarization components are characterized in the source rest reference frame by a constant frequency f_0, it is interesting to calculate the time scale during which such a periodic signal will still appear in the LISA data as a sinusoid. In the LISA reference frame, any of the TDI responses will measure a sinusoidal signal whose frequency is Doppler modulated by the LISA motion around the Sun in the following way:

$$f(t) = f_0\left[1 - \frac{\hat{k}\cdot\vec{V}(t)}{c}\right], \tag{25}$$

where $\hat{k}$ is the unit vector of propagation of the wave, $\vec{V}$ is the velocity of the LISA guiding center o relative to the solar system barycenter, and c is the speed of light [18,19]. If we take the root-mean-square (rms) value of the frequency change given by Eq. (25), averaged over all possible incoming directions of the GW signal, we obtain the following resulting rms value of the Doppler change of the signal frequency in the LISA reference frame:

$$\Delta f \equiv \langle (f(t) - f_0)^2\rangle^{1/2} = \pm f_0\frac{V_0}{2c}, \tag{26}$$

where V_0 is the velocity amplitude of the almost sinusoidal motion of the array around the Sun, and the angle brackets $\langle\,\rangle$ denote an ensemble average over source directions. If we take $V_0 \simeq 30$ km/s, and assume

$f_0 = 10^{-2}$ Hz, the corresponding rms frequency shift is equal to $\Delta f = 5.0 \times 10^{-7}$ Hz. In other words, if we would integrate the data for about 20 days, the data frequency resolution would be equal to or larger than the corresponding rms frequency shift induced by the Doppler modulation. Since the frequency shift induced by the amplitude modulation is smaller than the Doppler frequency modulation at this frequency f_0, ([18,19]), it follows that over a period of about 20 days, the expression of the ZSS can be used for identifying two points in the sky where an observed sinusoidal signal might have arrived from.

As an example, in Fig. 4(a) we plot contours of constant power spectral density of the ZSS in terms of its two parameters (θ, ϕ), in the case of a circularly polarized sinusoidal signal of frequency $f_0 = 10^{-2}$ Hz, incoming from $\theta_s = 32°$, $\phi_s = 107°$ and for noiseless data. Note that the ZSS is equal to zero only at the correct source location, and at its mirror image with respect to the LISA plane. Also, the plane of symmetry (defined by $\theta = 90°$) shows an identically null ZSS. This is because every TDI response is insensitive to the "×" polarization components of signals incoming from sources located in the LISA plane (see Appendix A). This makes the ZSS degenerate for these source directions. Figure 4(b) shows instead the power spectral density of the ZSS as a function of θ, for the cases $\phi = \phi_s = 107°$, and $\phi = 207°$, while in Fig. 4(c) we plot it as a function of ϕ and for the choices $\theta = \theta_s = 32°$, and $\theta = 59°$. From these two plots it is possible to have an idea of the sharpness and narrowness of the nulls in terms of the angles (θ, ϕ). In order to estimate the magnitude of the accuracy by which these two points in the sky can be identified with this method, however, it will be necessary to include the effects induced by the noises and the magnitude of the SNR by which the signal is detected in the three Sagnac observables (α, β, γ) [17]. This analysis will be presented in our forthcoming "part II" article.

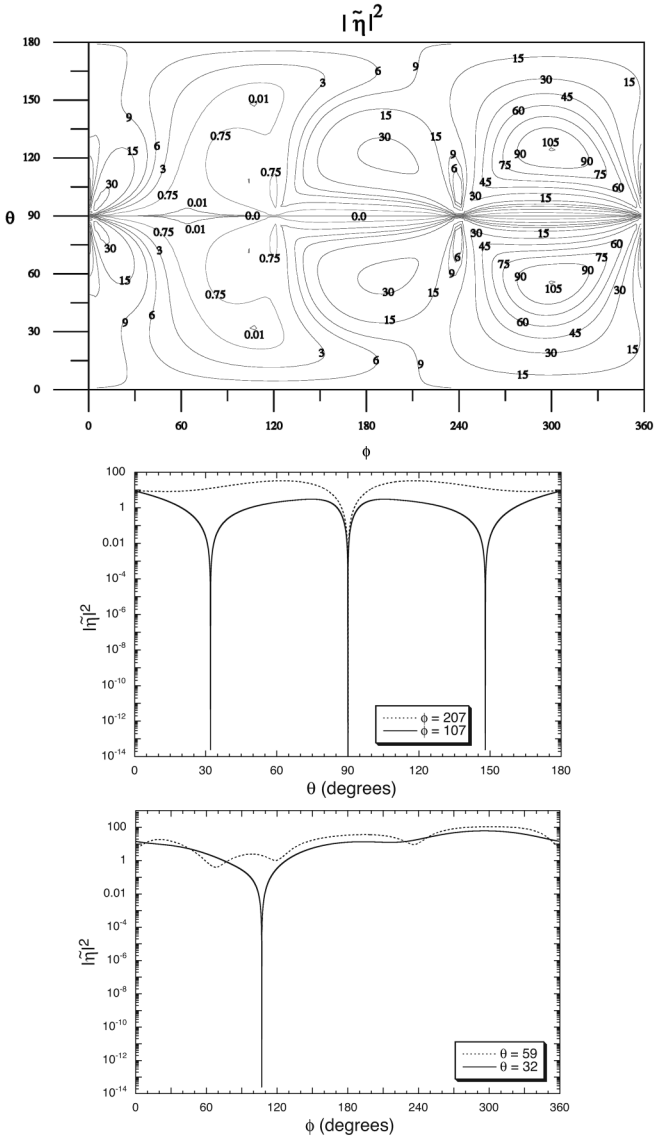

FIG. 4. (a) Contours of constant level of the modulus squared of the ZSS constructed for a sinusoidal signal of frequency $f_0 = 10^{-2}$ Hz, incoming from a source located at $\theta_s = 32°$, $\phi_s = 107°$. The plot is symmetric with respect to the LISA plane ($\theta = 90°$); (b) two cross sections along the θ axis of the modulus squared of the ZSS for the same signal of (a); one curve corresponds to $\phi = \phi_s = 107°$, and the other to $\phi = 207° \neq \phi_s$. (c) Two cross sections along the ϕ axis, with $\theta = \theta_s = 32°$, and $\theta = 59°$.

IV. THE ZSS IN THE TIME DOMAIN

The expression of the ZSS can also be given in the time domain by inverse Fourier transforming Eq. (24). Having the ZSS in the time domain will be particularly useful when attempting to discriminate gravitational wave bursts against statistically significant fluctuations generated by instrumental noise affecting the three TDI combinations (α, β, γ). A quantitative analysis of the improvement in statistical confidence added by using the ZSS as a veto against noise fluctuations will be addressed in a follow-up paper.

In order to derive the time-domain expression of the ZSS, let us consider only one of the three terms entering into the expression of the Fourier transform of the ZSS given in Eq. (24), say $a_3(f, \theta, \phi)\tilde{\gamma}(f)$. This is because the other two terms entering into the ZSS can be obtained from it by permuting the spacecraft indices.

Since the function $a_3(f, \theta, \phi)$ can be written in the following analytic form:

$$a_3(f, \theta, \phi) = \sum_{k=1}^{27} A_3^{(k)}(\theta, \phi) e^{2\pi i f \Delta_3^{(k)}}, \qquad (27)$$

where the 27 "amplitudes" $A_3^{(k)}$ and the corresponding

"delays" $\Delta_3^{(k)}$ depend only on the angles (θ, ϕ) and not on the Fourier frequency f, it follows from the linearity of the inverse-Fourier transform that the expression of the ZSS in the time domain assumes the following form:

$$\eta(t, \theta, \phi) = \sum_{k=1}^{27} [A_1^{(k)} \alpha(t - \Delta_1^{(k)}) + A_2^{(k)} \beta(t - \Delta_2^{(k)}) + A_3^{(k)} \gamma(t - \Delta_3^{(k)})]. \quad (28)$$

If we take into account that each of the Sagnac observable shows a gravitational wave pulse at six distinct times, we conclude that for an arbitrary pair (θ, ϕ), the ZSS will display in principle "486" pulses. At the correct source location, and at its mirror image with respect to the LISA plane, the ZSS becomes null, making all these pulses disappear.

Figures 5–7 schematically show the implementation of the ZSS in the case of a gravitational wave burst whose wave components, $h_+(t)$, $h_\times(t)$, are deltalike pulses of unit amplitudes. The noiseless responses of the three Sagnac combinations to such a gravitational wave signal, which we have assumed to be incoming from $(\theta_s = 32°, \phi_s = 107°)$, are given in Figs. 5(a)–5(c). Note the characteristic six-pulse structure of their responses. In Figs. 6(a)–6(c) the time-domain expressions of the inverse-Fourier transforms of the functions $a_1(f, \theta, \phi)\tilde{\alpha}(f)$, $a_2(f, \theta, \phi)\tilde{\beta}(f)$, $a_3(f, \theta, \phi)\tilde{\gamma}(f)$ are plotted for values of the angles $(\theta = 31.5°, \phi = 106.5°)$. The corresponding ZSS combination is given in Fig. 6(d), showing that no cancellation is achieved for values of the polar angles slightly different from those corresponding to the source location. Figures 7(a)–7(d) shows instead plots similar to those given by Fig. 6, but now with $(\theta, \phi) = (\theta_s, \phi_s)$.

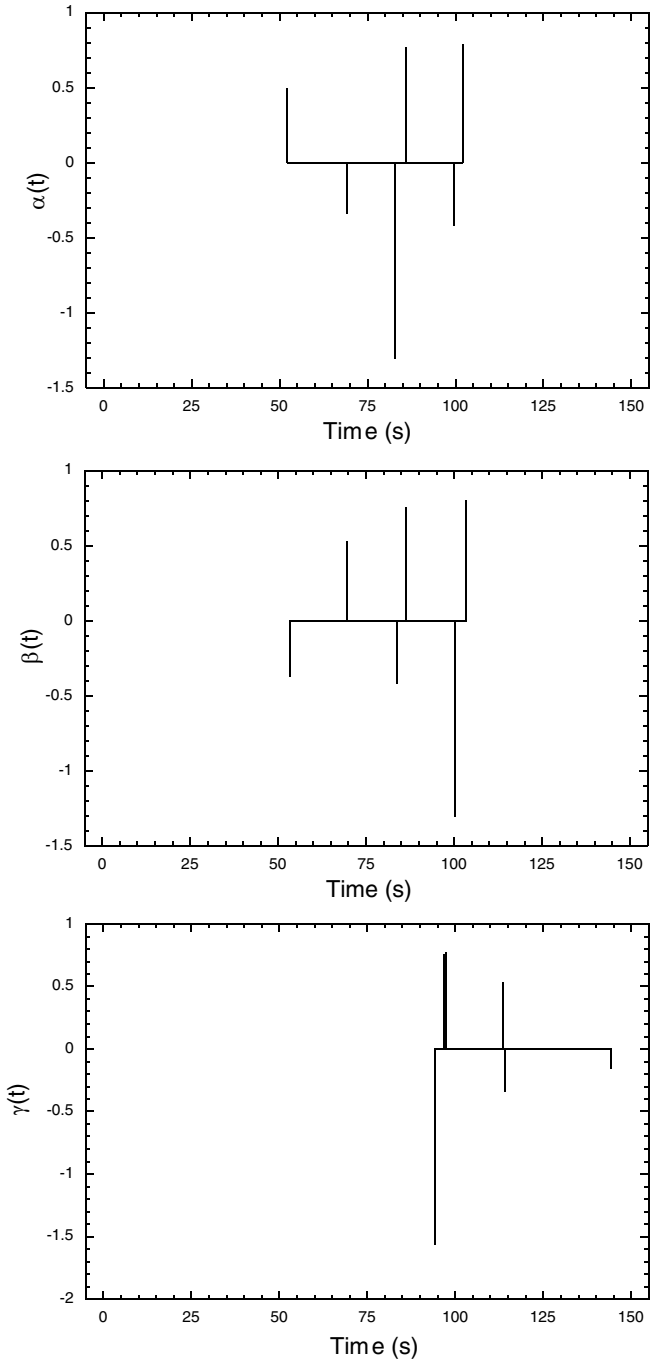

FIG. 5. The responses of the three Sagnac combinations, α (a), β (b), and γ (c), to a gravitational wave burst of unit amplitudes. The source has been assumed to be located at $\theta_s = 32°$, $\phi_s = 107°$.

V. THE LONG-WAVELENGTH LIMIT

In order to understand the behavior of the ZSS, η, in the low part of the LISA frequency band, we provide in this section its analytic expression in the long-wavelength limit (LWL), i.e., when the characteristic wavelength of the GW signal, λ, is much larger than the typical scale size of the array, L.

Let us rewrite the expression for η in the Fourier domain [see Eq. (24) above]

$$\begin{aligned}\tilde{\eta} \equiv & [\beta_+(f,\theta,\phi)\gamma_\times(f,\theta,\phi) - \beta_\times(f,\theta,\phi)\gamma_+(f,\theta,\phi)]\tilde{\alpha}(f) \\ & + [\gamma_+(f,\theta,\phi)\alpha_\times(f,\theta,\phi) \\ & - \gamma_\times(f,\theta,\phi)\alpha_+(f,\theta,\phi)]\tilde{\beta}(f) \\ & + [\alpha_+(f,\theta,\phi)\beta_\times(f,\theta,\phi) \\ & - \alpha_\times(f,\theta,\phi)\beta_+(f,\theta,\phi)]\tilde{\gamma}(f), \end{aligned} \quad (29)$$

where the functions α_+, $\alpha_\times$, β_+, $\beta_\times$, and γ_+, $\gamma_\times$ are given in Appendix B. We have been able to find the long-wavelength expansion $(fL \ll 1)$ of $\tilde{\eta}$ by using the program MATHEMATICA [20]. Since the LISA arm lengths will differ at most by a few percents [1], the general expression of the ZSS in the long-wavelength limit can be written in the following simpler form:

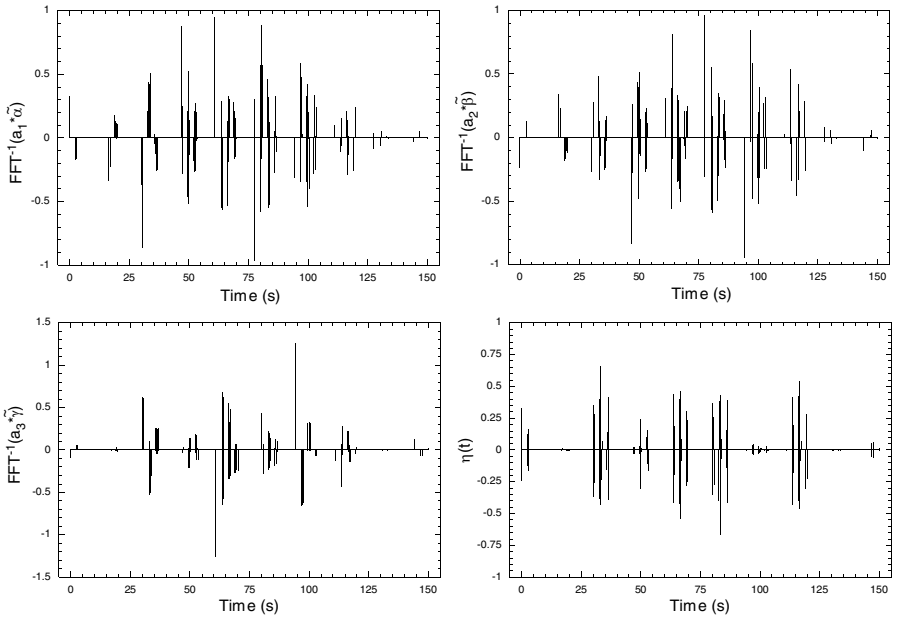

FIG. 6. The time-domain responses of the inverse-Fourier transforms of the three functions, $a_1\tilde{\alpha}$ (a), $a_2\tilde{\beta}$ (b), $a_3\tilde{\gamma}$ (c), which determine the ZSS. The angles (θ, ϕ), over which the search is performed have been fixed to be equal to $\theta = 31.5°$, $\phi = 106.5°$; (d) the ZSS constructed from the functions shown in (a)–(c).

$$\tilde{\eta}(f,\theta,\phi) \approx (2\pi f L)^4[(F_1^+F_2^\times - F_1^\times F_2^+) + (F_2^+F_3^\times - F_2^\times F_3^+) + (F_3^+F_1^\times - F_3^\times F_1^+)] \times \Big\{\frac{i(2\pi f L)^3}{4}(\hat{k}^{(s)} - \hat{k})\cdot[\hat{n}_1(\hat{n}_1\cdot\tilde{\mathbf{h}}^{(s)}(f)\cdot\hat{n}_1) + \hat{n}_2(\hat{n}_2\cdot\tilde{\mathbf{h}}^{(s)}(f)\cdot\hat{n}_2) + \hat{n}_3(\hat{n}_3\cdot\tilde{\mathbf{h}}^{(s)}(f)\cdot\hat{n}_3)] + \tilde{\alpha}_n + \tilde{\beta}_n + \tilde{\gamma}_n\Big\}, \tag{30}$$

where L is the nominal LISA arm length ($\simeq 5\times 10^6$ km), the label $^{(s)}$ on a specific functions means "evaluated at $\theta = \theta_s$; $\phi = \phi_s$," and $(\tilde{\alpha}_n, \tilde{\beta}_n, \tilde{\gamma}_n)$ are the Fourier transforms of the three random processes associated with the noises in (α, β, γ). Note that as $(k_x, k_y, \pm k_z) \to (k_x, k_y, \pm k_z)^{(s)}$, $\tilde{\eta} \to 0$ as expected. This is because the unit vector $\hat{k}$, corresponding to a point that is the mirror image of the source location relative to the

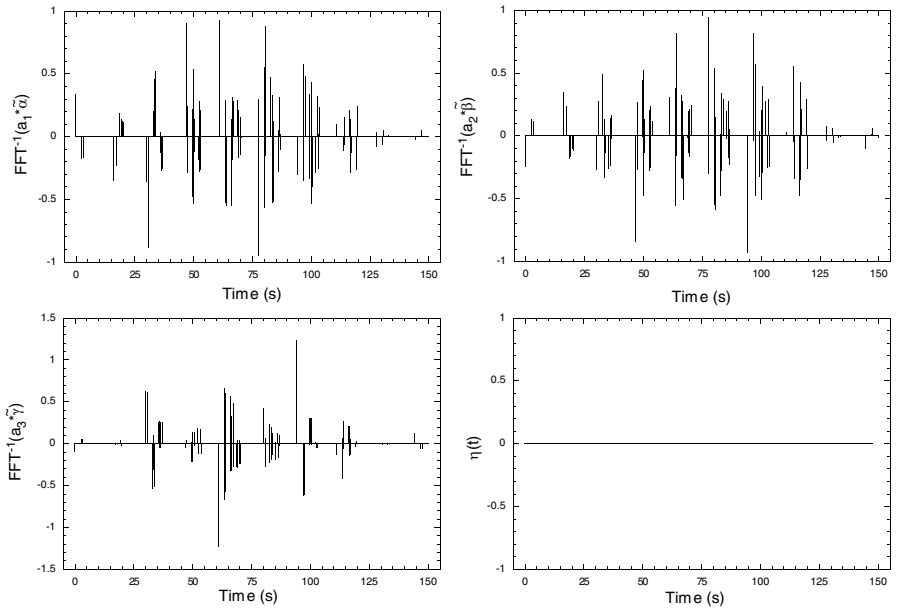

FIG. 7. Plots (a)–(d) are as in Fig. 6, but now with $(\theta = \theta_s, \phi = \phi_s)$.

LISA plane, will have the same scalar product with the three unit vectors $\hat{n}_j$ as $\hat{k}^{(s)}$.

It is interesting to compare the LWL expression of the ZSS given above, against that for the symmetric Sagnac combination, ζ [10]

$$\tilde{\zeta}^{gw}(f) \simeq \tfrac{1}{12}(2\pi i f L)^3\{(\hat{k}\cdot\hat{n}_1)[\hat{n}_1\cdot\tilde{\mathbf{h}}(f)\cdot\hat{n}_1] + (\hat{k}\cdot\hat{n}_2)[\hat{n}_2\cdot\tilde{\mathbf{h}}(f)\cdot\hat{n}_2] + (\hat{k}\cdot\hat{n}_3)[\hat{n}_3\cdot\tilde{\mathbf{h}}(f)\cdot\hat{n}_3]\} + \tfrac{1}{3}[\tilde{\alpha}_n + \tilde{\beta}_n + \tilde{\gamma}_n], \tag{31}$$

where the noise affecting ζ can be rewritten (in the LWL) in terms of the (α, β, γ) noises by using the LWL limit of the Fourier transform of Eq. (6) with equal-arm lengths. Although both combinations display the $(2\pi f L)^3$ dependence in the signal and the same noises, the ability of $\tilde{\eta}$ to further suppress the gravitational wave signal by identifying the direction it came from should be regarded as an improvement over ζ. This property will be particularly useful for discriminating exceptionally strong signals against random noise fluctuations that will be still observable by ζ in this low part of the LISA frequency band.

VI. SUMMARY AND CONCLUSIONS

We have identified a method for nulling a gravitational wave signal observed in coincidence by three LISA TDI combinations. We have named the resulting TDI combination the zero-signal solution. The method can in principle identify two points in the sky where a gravitational wave burst, or a sinusoidal signal, came from. In order for the method to work in the case of a sinusoidal signal, the gravitational wave signal must be observable after integrating the data over a period such that the Doppler modulation induced by the LISA motion around the Sun can be disregarded.

Although the analytic expression of the ZSS has been derived in terms of the three Sagnac observables (α, β, γ), any other three TDI combinations capable of generating the entire TDI space (such as the unequal-arm Michelson combinations X, Y, Z) could have been used. In particular, the TDI combinations (A, E, T) [11], whose noises are uncorrelated, would have worked as well. The use of the (A, E, T) combinations will be particularly useful when we will estimate the accuracies provided by the ZSS in determining the source location and the wave's two amplitudes. These points will be addressed in our follow-up article.

ACKNOWLEDGMENTS

S. L. L. acknowledges support from LISA Contract No. PO 1217163. The research was performed at the Jet Propulsion Laboratory, California Institute of Technology, under contract with the National Aeronautics and Space Administration.

APPENDIX A: THE BEAM-PATTERN FUNCTIONS

This appendix derives the analytic expressions of the antenna patterns $F_j^+(\theta, \phi)$, $F_j^\times(\theta, \phi)$ entering in the wave functions $\Psi_j(t)$, $j = 1, 2, 3$, and in the pattern functions α_+, $\alpha_\times$, β_+, $\beta_\times$, γ_+, $\gamma_\times$ introduced in Eqs. (15)–(17), and given in Appendix B.

Consider a plane gravitational wave of direction of propagation $\hat{k}$ incident on the LISA spacecraft constellation. Let the wave coordinate system be (x', y', z'), with the wave traveling in the z' direction, and let the axes with respect to which $h_+(t)$, and $h_\times(t)$ are referred to be the (x', y') axes. The coordinate system associated with LISA, (x, y, z) is obtained from them by a rotation described by the polar angles (θ, ϕ) (Fig. 3). For sake of simplicity, and without lack of generality, we can assume the x' axis to be parallel to the (x, y) plane, and the wave's two independent amplitudes $h_+(t)$, and $h_\times(t)$, associated with the two independent polarizations, to be defined with respect to this choice of coordinates.

Let us now consider the null vector $\vec{m}$ defined by

$$\vec{m} \equiv \frac{1}{\sqrt{2}}(\hat{e}_{x'} + i\hat{e}_{y'}), \tag{A1}$$

where $\hat{e}_{x'}$, $\hat{e}_{y'}$ are the unit vectors in the x', y' directions, respectively. The tensor $\mathbf{h}$ is then just [17]

$$\mathbf{h} = 2h_+(t)\mathrm{Re}(\vec{m}\otimes\vec{m}) + 2h_\times(t)\mathrm{Im}(\vec{m}\otimes\vec{m}). \tag{A2}$$

In the LISA coordinate system the components of h_{ij} can be obtained by finding the components of $\vec{m}$ in these coordinates. The vector $\vec{m}$ can be written as

$$\vec{m} = \frac{1}{\sqrt{2}}[(-\sin\phi + i\cos\theta\cos\phi)\hat{e}_x + (\cos\phi + i\cos\theta\sin\phi)\hat{e}_y + (i\sin\theta)\hat{e}_z], \tag{A3}$$

while the unit vector $\hat{k}$, describing the direction of propagation of the wave from the source to LISA assumes the following form:

$$\hat{k} = (-\sin\theta\cos\phi)\hat{e}_x + (-\sin\theta\sin\phi)\hat{e}_y + (-\cos\theta)\hat{e}_z. \tag{A4}$$

Since the $\Psi_j(t)$, $j = 1, 2, 3$ functions, entering into the expressions of α^{gw}, β^{gw}, γ^{gw} have the following analytic forms:

$$\Psi_j(t) = \frac{1}{2}\frac{\hat{n}_j\cdot\mathbf{h}(t)\cdot\hat{n}_j}{1-(\hat{k}\cdot\hat{n}_j)^2}, \tag{A5}$$

after replacing Eq. (A2) into (A5), and performing some simple algebra, we can rewrite $\Psi_j(t)$ in the following form:

$$\Psi_j(t) \equiv \frac{F_j^+(\theta,\phi)h_+(t) + F_j^\times(\theta,\phi)h_\times(t)}{2[1-(\hat{k}\cdot\hat{n}_j)^2]}, \tag{A6}$$

where the functions $F_j^+(\theta,\phi)$, $F_j^\times(\theta,\phi)$ are equal to

$$F_j^+(\theta,\phi) \equiv 2[\hat{n}_j \cdot \mathrm{Re}(\vec{m}\otimes\vec{m})\cdot\hat{n}_j], \tag{A7}$$

$$F_j^\times(\theta,\phi) \equiv 2[\hat{n}_j \cdot \mathrm{Im}(\vec{m}\otimes\vec{m})\cdot\hat{n}_j]. \tag{A8}$$

If we now rewrite the vector $\vec{m}$ in the following form:

$$\vec{m} \equiv \vec{m}_1 + i\vec{m}_2, \tag{A9}$$

where the two vectors $\vec{m}_1$, $\vec{m}_2$ have components

$$\vec{m}_1 = \frac{1}{\sqrt{2}}[(-\sin\phi)\hat{e}_x + (\cos\phi)\hat{e}_y],$$
$$\vec{m}_2 = \frac{1}{\sqrt{2}}[(\cos\theta\cos\phi)\hat{e}_x + (\cos\theta\sin\phi)\hat{e}_y + (\sin\theta)\hat{e}_z], \tag{A10}$$

the tensor product $\vec{m}\otimes\vec{m}$ becomes equal to

$$\vec{m}\otimes\vec{m} = [(\vec{m}_1\otimes\vec{m}_1) - (\vec{m}_2\otimes\vec{m}_2)] + i[(\vec{m}_1\otimes\vec{m}_2) + (\vec{m}_2\otimes\vec{m}_1)]. \tag{A11}$$

The expressions for F_j^+, $F_j^\times$ given in Eqs. (A7) and (A8) can be rewritten as

$$F_j^+ = 2[(\hat{n}_j\cdot\vec{m}_1)^2 - (\hat{n}_j\cdot\vec{m}_2)^2], \tag{A12}$$

$$F_j^\times = 4(\hat{n}_j\cdot\vec{m}_1)(\hat{n}_j\cdot\vec{m}_2), \qquad j=1,2,3. \tag{A13}$$

Since the unit vectors $\hat{n}_j$ are in the (x, y) plane, they can be expressed as

$$\hat{n}_j = \cos(\nu_j)\hat{e}_x + \sin(\nu_j)\hat{e}_y, \qquad j=1,2,3, \tag{A14}$$

and Eqs. (A12) and (A13), after some simple algebra, assume the following form:

$$F_j^+ = [\sin^2(\nu_j-\phi) - \cos^2(\nu_j-\phi)\cos^2\theta], \tag{A15}$$

$$F_j^\times = [\cos\theta\sin 2(\nu_j-\phi)], \qquad j=1,2,3. \tag{A16}$$

Equations (A15) and (A16) show that the F_j^+ beam-pattern functions are invariant under the transformation $\theta\to\pi-\theta$, while the $F_j^\times$ change sign. These symmetry properties of the $F_j^{+,\times}$ functions imply that the ZSS changes sign under the same transformation, an important property highlighted in Sec. II.

APPENDIX B: THE ZSS COEFFICIENTS a_1, a_2, a_3

In order to derive the expression of the ZSS in the Fourier domain we have introduced the *generalized beam-pattern functions* α_+, $\alpha_\times$, β_+, $\beta_\times$, and γ_+, $\gamma_\times$ [see Eqs. (15)–(17)], while the corresponding expression in the time domain [Eq. (27)] was written in terms of 81 amplitudes, $A_j^{(k)}$, and corresponding time delays, $\Delta_j^{(k)}$, $j=1,2,3$, $k=1,2,\ldots,27$. In this appendix we provide the analytic expressions of these functions.

Using the identities $\mu_i = \vec{k}\cdot\hat{p}_i$ and

$$w_1 \equiv \hat{k}\cdot\hat{n}_1 = \frac{\ell}{L_1}(\mu_2-\mu_3), \tag{B1}$$

$$w_2 \equiv \hat{k}\cdot\hat{n}_2 = \frac{\ell}{L_2}(\mu_3-\mu_1), \tag{B2}$$

$$w_3 \equiv \hat{k}\cdot\hat{n}_3 = \frac{\ell}{L_3}(\mu_1-\mu_2), \tag{B3}$$

the signal part of $\alpha(t)$ is written in the time domain as

$$\alpha^{gw} = [1-w_2][\Psi_2(t-L_2-\mu_3\ell) - \Psi_2(t-\mu_1\ell)] - [1+w_2][\Psi_2(t-L_1-L_2-L_3-\mu_1\ell) - \Psi_2(t-L_1-L_3-\mu_3\ell)] + [1-w_3][\Psi_3(t-L_1-L_2-L_3-\mu_1\ell) - \Psi_3(t-L_1-L_2-\mu_2\ell)] - [1+w_3][\Psi_3(t-L_3-\mu_2\ell) - \Psi_3(t-\mu_1\ell)] + [1-w_1][\Psi_1(t-L_1-L_2-\mu_2\ell) - \Psi_1(t-L_2-\mu_3\ell)] - [1+w_1][\Psi_1(t-L_1-L_3-\mu_3\ell) - \Psi_1(t-L_3-\mu_2\ell)]. \tag{B4}$$

Since in the frequency domain the functions Ψ_i are equal to

$$\tilde{\Psi}_i = \frac{F_i^+\tilde{h}_+ + F_i^\times\tilde{h}_\times}{2(1-w_i^2)}, \tag{B5}$$

the response of the interferometric variable α, to a gravitational wave signal, becomes

$$\tilde{\alpha}(f) = \alpha_+(f,\theta,\phi)\tilde{h}_+ + \alpha_\times(f,\theta,\phi)\tilde{h}_\times, \tag{B6}$$

where the coefficients $\alpha_{+,\times}(f,\theta,\phi)$ may be written as

$$\alpha_{+,\times}(f,\theta,\phi) = \alpha_1 F_1^{+,\times} + \alpha_2 F_2^{+,\times} + \alpha_3 F_3^{+,\times}. \tag{B7}$$

In Eq. (B7) the functions α_1, α_2, α_3 are given by the following expressions:

$$\alpha_1 = \frac{(e^{i2\pi f(L_1+L_2+\mu_2\ell)} - e^{i2\pi f(L_2+\mu_3\ell)})}{2(1+w_1)} + \frac{(e^{i2\pi f(L_3+\mu_2\ell)} - e^{i2\pi f(L_1+L_3+\mu_3\ell)})}{2(1-w_1)}, \tag{B8}$$

$$\alpha_2 = \frac{(e^{i2\pi f(L_2+\mu_3\ell)} - e^{i2\pi f(\mu_1\ell)})}{2(1+w_2)} + \frac{(e^{i2\pi f(L_1+L_3+\mu_3\ell)} - e^{i2\pi f(L_1+L_2+L_3+\mu_1\ell)})}{2(1-w_2)}, \tag{B9}$$

$$\alpha_3 = \frac{(e^{i2\pi f(L_1+L_2+L_3+\mu_1\ell)} - e^{i2\pi f(L_1+L_2+\mu_2\ell)})}{2(1+w_3)} + \frac{(e^{i2\pi f(\mu_1\ell)} - e^{i2\pi f(L_3+\mu_2\ell)})}{2(1-w_3)}. \quad \text{(B10)}$$

The numerical indices are again spacecraft indices, which can be permuted in order to obtain the corresponding functions for the other TDI combinations β, and γ (indices $1 \to 2 \to 3 \to 1$, such that $\alpha \to \beta \to \gamma \to \alpha$).

The a_3 coefficient in the zero-signal solution is built from combinations of the pattern functions that determine the responses of $\tilde{\alpha}$ and $\tilde{\beta}$ to the gravitational wave signal. Its analytic expression can now be rewritten as

$$\begin{aligned} a_3 &= \alpha_+\beta_\times - \alpha_\times\beta_+ \\ &= (\alpha_1\beta_2 - \alpha_2\beta_1)(F_1^+F_2^\times - F_1^\times F_2^+) \\ &\quad + (\alpha_3\beta_1 - \alpha_1\beta_3)(F_3^+F_1^\times - F_3^\times F_1^+) \\ &\quad + (\alpha_2\beta_3 - \alpha_3\beta_2)(F_2^+F_3^\times - F_2^\times F_3^+). \end{aligned} \quad \text{(B11)}$$

After algebraically expanding the expression above we can rewrite a_3 in the following form:

$$a_3 = \sum_{k=1}^{27} A_3^{(k)} e^{2\pi i f \Delta_3^{(k)}}, \quad \text{(B12)}$$

where the $\Delta_3^{(k)}$ are 27 different time shifts associated with the coefficient a_3, and the $A_3^{(k)}$ are functions that only depend on the geometric angles (θ, ϕ). Since there are 27 unique time delays associated with each of the $\{a_i\}$ coefficients, and because the gravitational wave signal enters in each TDI variable at six different times (the so-called six-pulse response), it follows that in general the ZSS will display a total of "$3 \times (6 \times 27) = 486$ pulses." At the correct source location of course all these pulses add up to zero.

The analytic expressions for the 27 time delays entering into a_3 are given in the Table I. The remaining 54 can be obtained from them by making a permutation over the spacecraft indices.

Finally, the functions $A_3^{(k)}$, introduced in Eq. (B12), can be written in the following form:

$$\begin{aligned} A_3^{(k)} = [&\Upsilon_{12}^{(k)}(F_1^+F_2^\times - F_1^\times F_2^+) + \kappa_{31}^{(k)}(F_3^+F_1^\times - F_3^\times F_1^+) \\ &+ \chi_{23}^{(k)}(F_2^+F_3^\times - F_2^\times F_3^+)], \end{aligned} \quad \text{(B13)}$$

where the functions $\Upsilon_{12}^{(k)}$, $\kappa_{31}^{(k)}$, $\chi_{23}^{(k)}$ are

$$\Upsilon_{12}^{(1)} = -\Upsilon_{12}^{(2)} = \frac{w_1 - w_2}{2(1-w_1^2)(1-w_2^2)}, \quad \text{(B14)}$$

$$\begin{aligned} \Upsilon_{12}^{(3)} &= \Upsilon_{12}^{(6)} = \Upsilon_{12}^{(8)} = -\Upsilon_{12}^{(4)} = -\Upsilon_{12}^{(5)} = -\Upsilon_{12}^{(7)} \\ &= \frac{1}{4(1-w_1)(1+w_2)}, \end{aligned} \quad \text{(B15)}$$

$$\begin{aligned} \Upsilon_{12}^{(9)} &= \Upsilon_{12}^{(13)} = \Upsilon_{12}^{(14)} = -\Upsilon_{12}^{(10)} = -\Upsilon_{12}^{(11)} = -\Upsilon_{12}^{(12)} \\ &= \frac{1}{4(1+w_1)(1-w_2)}, \end{aligned} \quad \text{(B16)}$$

$$\begin{aligned} \Upsilon_{12}^{(15)} &= \Upsilon_{12}^{(16)} = \Upsilon_{12}^{(17)} = \Upsilon_{12}^{(18)} = \Upsilon_{12}^{(19)} = \Upsilon_{12}^{(20)} = \Upsilon_{12}^{(21)} \\ &= \Upsilon_{12}^{(22)} = \Upsilon_{12}^{(23)} = \Upsilon_{12}^{(24)} = \Upsilon_{12}^{(25)} = \Upsilon_{12}^{(26)} = \Upsilon_{12}^{(27)} \\ &= 0, \end{aligned} \quad \text{(B17)}$$

$$\kappa_{31}^{(3)} = -\kappa_{31}^{(5)} = -\kappa_{31}^{(12)} = \frac{1}{4(1-w_1)(1-w_3)}, \quad \text{(B18)}$$

$$\kappa_{31}^{(4)} = -\kappa_{31}^{(6)} = -\kappa_{31}^{(14)} = -\frac{1}{4(1-w_1)(1+w_3)}, \quad \text{(B19)}$$

$$\kappa_{31}^{(7)} = \kappa_{31}^{(11)} = -\kappa_{31}^{(9)} = -\frac{1}{4(1+w_1)(1+w_3)}, \quad \text{(B20)}$$

$$\kappa_{31}^{(8)} = \kappa_{31}^{(13)} = -\kappa_{31}^{(10)} = \frac{1}{4(1+w_1)(1-w_3)}, \quad \text{(B21)}$$

TABLE I. The 27 time delays entering into the function a_3, which multiplies the Fourier transform of the measurement γ. The other 54 time delays, entering into the functions a_1 and a_2, can be obtained by permuting, once and twice, respectively, the spacecraft indices of the expressions below.

k	$\Delta_3^{(k)}$	k	$\Delta_3^{(k)}$	k	$\Delta_3^{(k)}$
1	$L_1 + L_2 + 2l\mu_3$	10	$2L_1 + 2L_2 + l(\mu_1 + \mu_2)$	19	$L_3 + 2l\mu_2$
2	$L_1 + L_2 + 2L_3 + 2l\mu_3$	11	$L_1 + 2L_2 + 2L_3 + l(\mu_1 + \mu_3)$	20	$2L_1 + L_2 + L_3 + l(\mu_1 + \mu_3)$
3	$l(\mu_1 + \mu_2)$	12	$2L_1 + L_2 + 2L_3 + l(\mu_2 + \mu_3)$	21	$L_1 + L_3 + l(\mu_2 + \mu_3)$
4	$2L_3 + l(\mu_1 + \mu_2)$	13	$L_1 + 2L_2 + l(\mu_1 + \mu_2)$	22	$L_1 + L_2 + 2l\mu_2$
5	$L_1 + l(\mu_1 + \mu_3)$	14	$2L_1 + L_2 + l(\mu_2 + \mu_3)$	23	$L_1 + L_2 + 2L_3 + 2l\mu_2$
6	$L_1 + 2L_3 + l(\mu_1 + \mu_3)$	15	$L_1 + L_2 + L_3 + l(\mu_1 + \mu_2)$	24	$L_3 + 2l\mu_1$
7	$L_2 + l(\mu_2 + \mu_3)$	16	$2L_1 + 2L_2 + L_3 + 2l\mu_2$	25	$2L_1 + 2L_2 + L_3 + 2l\mu_1$
8	$L_2 + 2L_3 + l(\mu_2 + \mu_3)$	17	$L_1 + 2L_2 + L_3 + l(\mu_2 + \mu_3)$	26	$L_1 + L_2 + 2L_3 + 2l\mu_1$
9	$2L_1 + 2L_2 + 2L_3 + l(\mu_1 + \mu_2)$	18	$L_2 + L_3 + l(\mu_1 + \mu_3)$	27	$L_1 + L_2 + 2l\mu_1$

$$\kappa_{31}^{(15)} = -\frac{w_1 w_3}{(1-w_1^2)(1-w_3^2)}, \tag{B22}$$

$$\kappa_{31}^{(16)} = -\kappa_{31}^{(17)} = -\kappa_{31}^{(18)} = \frac{w_3}{2(1+w_1)(1-w_3^2)}, \tag{B23}$$

$$\kappa_{31}^{(19)} = -\kappa_{31}^{(20)} = -\kappa_{31}^{(21)} = -\frac{w_3}{2(1-w_1)(1-w_3^2)}, \tag{B24}$$

$$\kappa_{31}^{(22)} = -\frac{w_1}{2(1-w_1^2)(1+w_3)}, \tag{B25}$$

$$\kappa_{31}^{(23)} = \frac{w_1}{2(1-w_1^2)(1-w_3)}, \tag{B26}$$

$$\kappa_{31}^{(1)} = \kappa_{31}^{(2)} = \kappa_{31}^{(24)} = \kappa_{31}^{(25)} = \kappa_{31}^{(26)} = \kappa_{31}^{(27)} = 0, \tag{B27}$$

$$\chi_{23}^{(3)} = -\chi_{23}^{(7)} = -\chi_{23}^{(11)} = \frac{1}{4(1+w_2)(1+w_3)}, \tag{B28}$$

$$\chi_{23}^{(4)} = -\chi_{23}^{(8)} = -\chi_{23}^{(13)} = -\frac{1}{4(1+w_2)(1-w_3)}, \tag{B29}$$

$$\chi_{23}^{(5)} = \chi_{23}^{(12)} = -\chi_{23}^{(9)} = -\frac{1}{4(1-w_2)(1-w_3)}, \tag{B30}$$

$$\chi_{23}^{(6)} = \chi_{23}^{(14)} = -\chi_{23}^{(10)} = \frac{1}{4(1-w_2)(1+w_3)}, \tag{B31}$$

$$\chi_{23}^{15} = \frac{-w_2 w_3}{(1-w_2^2)(1-w_3^2)}, \tag{B32}$$

$$\chi_{23}^{(17)} = \chi_{23}^{(18)} = -\chi_{23}^{(24)} = -\frac{w_3}{2(1+w_2)(1-w_3^2)}, \tag{B33}$$

$$\chi_{23}^{20} = \chi_{23}^{21} = -\chi_{23}^{25} = \frac{w_3}{2(1-w_2)(1-w_3^2)}, \tag{B34}$$

$$\chi_{23}^{26} = -\frac{w_2}{2(1-w_2^2)(1+w_3)}, \tag{B35}$$

$$\chi_{23}^{27} = \frac{w_2}{2(1-w_2^2)(1-w_3)}, \tag{B36}$$

$$\chi_{23}^{(1)} = \chi_{23}^{(2)} = \chi_{23}^{(16)} = \chi_{23}^{(19)} = \chi_{23}^{(22)} = \chi_{23}^{(23)} = 0. \tag{B37}$$

[1] P. Bender, K. Danzmann, and the LISA Study Team, Max-Planck-Institüt für Quantenoptik Report No. MPQ233, 1998.
[2] J.W. Armstrong, F. B. Estabrook, and M. Tinto, Astrophys. J. **527**, 814 (1999).
[3] F. B. Estabrook, M. Tinto, and J.W. Armstrong, Phys. Rev. D **62**, 042002 (2000).
[4] M. Tinto, F. B. Estabrook, and J.W. Armstrong, Phys. Rev. D **65**, 082003 (2002).
[5] S.V. Dhurandhar, K. R. Nayak, and J.-Y. Vinet, Phys. Rev. D **65**, 102002 (2002).
[6] D. A. Shaddock, Phys. Rev. D **69**, 022001 (2004).
[7] N. J. Cornish and R.W. Hellings, Classical Quantum Gravity **20**, 4851 (2003).
[8] D. A. Shaddock, M. Tinto, F. B. Estabrook, and J.W. Armstrong, Phys. Rev. D **68**, 061303(R) (2003).
[9] M. Tinto, F. B. Estabrook, and J.W. Armstrong, Phys. Rev. D **69**, 082001 (2004).
[10] M. Tinto, J.W. Armstrong, and F. B. Estabrook, Phys. Rev. D **63**, 021101(R) (2000).
[11] T. A. Prince, M. Tinto, S. L. Larson, and J.W. Armstrong, Phys. Rev. D **66**, 122002 (2002).
[12] C. Cutler and Kip S. Thorne, gr-qc/0204090.
[13] M. Tinto and J.W. Armstrong, Phys. Rev. D **59**, 102003 (1999).
[14] In the literature [8], (ρ_1, ρ_2, ρ_3) are denoted $(\alpha_1, \alpha_2, \alpha_3)$. In order to avoid confusion with the notation introduced in Appendix A, we will use the symbols (ρ_1, ρ_2, ρ_3) for indicating the TDI2 Sagnac observables.
[15] J. Sylvestre and M. Tinto, Phys. Rev. D **68**, 102002 (2003).
[16] K. R. Nayak, S.V. Dhurandhar, A. Pai, and J.-Y. Vinet, Phys. Rev. D **68**, 122001 (2003).
[17] Y. Gürsel and M. Tinto, Phys. Rev. D **40**, 3884 (1989).
[18] N. Cornish and L. Rubbo, Phys. Rev. D **67**, 022001 (2003).
[19] A. Krolak, M. Tinto, and M. Vallisneri, Phys. Rev. D (to be published).
[20] S. Wolfram, *Mathematica: User Manual* (Wolfram Research, Inc., Redwood City, CA, 2002).